IET Generation, Transmission & Distribution

Research Article

IET Journals
The Institution of Engineering and Technology

Robust reactive power optimisation and voltage control method for active distribution networks via dual time-scale coordination

ISSN 1751-8687
Received on 21st June 2016
Revised 17th December 2016
Accepted on 14th January 2017
E-First on 31st March 2017
doi: 10.1049/iet-gtd.2016.0950
www.ietdl.org

Weiye Zheng[1], Wenchuan Wu[1] ✉, Boming Zhang[1], Yongjie Wang[1]

[1]*Department of Electrical Engineering, Tsinghua University, Beijing, People's Republic of China*

✉ *E-mail: wuwench@tsinghua.edu.cn*

Abstract: In distribution networks, there are slow controlling devices and fast controlling devices for Volt-VAr regulation. These slow controlling devices, such as capacitors or voltage regulators, cannot be operated frequently and should be scheduled tens of minutes ahead (hereafter named as slow control). Since of the uncertainties in predicting the load and distributed generation, the voltage violations cannot be eliminated by fast controlling devices with improper schedule of the slow controlling devices. In this paper we propose dual time-scale coordination for the Volt-VAr control scheme, corresponding to slow and fast control. Slow control guarantees that subsequent fast controls can maintain the system's voltage security if the uncertain parameters vary within predefined limits. A column-and-constraint generation algorithm was used to solve the robust convexified model. A conventional deterministic optimization model can be used to determine the fast control mechanism. The simulation results show that solving the deterministic model is not always feasible and voltage violation may occur. The robust model was shown to be effective with respect to all possible scenarios in the uncertainty set, with little compromise in terms of network losses.

Nomenclature

The main symbols used throughout this paper are stated below for quick reference. Others are defined as required.

Indices and sets

i, j	indices of buses, from 1 to N
ϕ	indices of phases, typically referring to a, b and c
t	iteration of the proposed algorithm
k	index of the tap settings of voltage regulators, from 1 to R
$\mathcal{N}$	set of buses in the entire system
$\mathcal{E}$	set of branches in the entire system
$\mathcal{K}_{ij}$	set of allowable taps of branch ij, consisting of $\{K_{ij,1}, K_{ij,2}, \ldots, K_{ij,R}\}$
$\mathcal{B}_i$	set of allowable on–off decisions for capacitor banks at bus i
$\mathcal{X}$	feasible region of the first-stage variables
$\mathcal{VR}$	set of branches with voltage regulators
$\mathcal{MSC}$	set of buses with mechanically switched capacitors/ capacitor banks
$\mathcal{D}$	uncertainty set for fluctuation of $\boldsymbol{d}$

Input parameters and functions

r_{ij}, x_{ij}	resistance and reactance of branch ij, respectively
V_{ref}	voltage at the point of common coupling
$\bar{I}_{ij}$	upper bound of the current magnitude of branch ij
$\bar{V}_i, \underline{V}_i$	upper and lower bounds of the voltage magnitude at bus i, respectively
$\bar{Q}_{\text{C}i}, \underline{Q}_{\text{C}i}$	upper and lower bounds of the injected reactive powers of the static VAr compensation devices at bus i, respectively
$\bar{Q}_{\text{G}i}, \underline{Q}_{\text{G}i}$	upper and lower bounds of the injected reactive powers of the generators at bus i, respectively
$\bar{b}_i^{\text{C}}$	the admittance element of capacitor bank at bus i
$\boldsymbol{d}_0$	forecasted loads and active outputs of DGs
$\boldsymbol{d}$	realised loads and active outputs of DGs

Variables

P_{ij}, Q_{ij}, l_{ij}	active power flow, reactive power flow and squared magnitude of the current at the sending end of branch ij, respectively
$P_{\text{D}i}, Q_{\text{D}i}$	active and reactive power load demands at bus i, respectively
$P_{\text{G}i}, Q_{\text{G}i}$	injected active and reactive powers of generators at bus i
$Q_{\text{C}i}$	total reactive power from compensators at bus i
v_i	squared voltage magnitude at bus i
P_i, Q_i	total injected active and reactive powers at bus i
κ_{ij}	turn ratio variable for tap changer at branch ij
β_i	on-and-off decision variable for the capacitor bank at bus i
$\boldsymbol{\beta}$	on-and-off decision vector for capacitor banks
$\boldsymbol{\kappa}$	tap setting vector for voltage regulators
$\boldsymbol{x}$	first-stage decision vector for voltage regulators and capacitor banks
$\boldsymbol{y}$	second-stage decision vector for reactive outputs of static VAr compensators and distributed generators

Notations: Upper (lower) boldface letters will be used for matrices (column vectors); $\|\cdot\|_p$ denotes the vector p-norm for $p \geq 1$; $(\cdot)^{\text{T}}$ transposition; $\boldsymbol{I}$ the identity matrix; variables with superscript φ denote corresponding variables for phase φ.

1 Introduction

Volt–VAr optimisation (VO) aims to minimise network power losses and prevent voltage violations by dispatching reactive power control devices [1]. In recent years, the numbers of renewable distributed generations (DGs) including photovoltaic (PV) and wind power generators have increased significantly in distribution networks, formulating active distribution networks (ADNs). Owing to the reverse power flow, DG outputs may lead to overvoltage [2]. To address this issue, reactive power optimisation was investigated in [3], in which it was shown that power losses can be reduced significantly. Most studies concerning reactive power optimisation do not consider any uncertain factors [4–6].

Three major factors contribute to the uncertainties in ADNs:

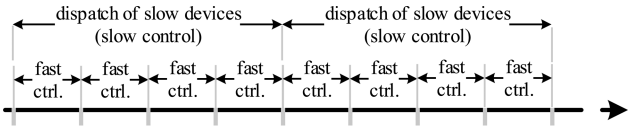

Fig. 1 *Timeline for sequential coordination of slow control and fast control*

i. The active outputs of renewable DGs fluctuate dramatically due to their inherent volatility and intermittency.
ii. Load demands vary with time and are hard to predict precisely.
iii. There are limited real-time measurements in distribution networks, so large errors may occur in the estimations of the outputs of the DGs and load demands.

These uncertainties pose a series of technical challenges to the operation of ADNs. Voltage regulation in distribution networks is conventionally accomplished by voltage regulators (VRs), under-load tap changing (ULTCs) transformers and capacitor banks/mechanically switched capacitors (MSCs). Although these devices are effective in managing slow variations in voltages, on the time-scale of hours, they do not perform well for fast fluctuations, on the time-scale of minutes or seconds.

On the one hand, these slow controlling devices cannot be operated frequently and they are expected to maintain their states for a long time, since the maximum allowable daily operating time (MADPT) is limited by the expected lifetime. On the other hand, in certain scenarios, where the actual loads and outputs of the DGs significantly deviate from their predicted values, voltage violation may occur. Some recent papers have made effort to address these uncertainties. On the basis of Niederreiter's quasi-random sampling technique, Saric *et al.* of [7] proposed a robust algorithm for volt–VAr control. However, optimality is not guaranteed by the theory. A robust voltage control model is described in [8], where a scenario generation and reduction method is used, but slow controlling devices such as ULTCs and MSCs are not considered. On the basis of scenario generation and reduction method, Daratha *et al.* [9] proposed a robust voltage regulation method, where monotonicity assumption is necessary for scenario reduction. Also, the discrete variables introduced by ULTCs and MSCs are tackled with an empirical two-step solution method.

Bus injection model (BIM) is a canonical model for power flow optimisation, which focuses on nodal variables [10]. On the basis of this formulation, semi-definite relaxation (SDR) has been proposed to transform the non-convex optimal power flow problem into convex one [11–13]. However, as investigated by Lesieutre *et al.* [13], SDR method has its limitation and sometimes leads to impractical solutions. Therefore, another formulation for optimal power flow problem in distribution networks is the branch flow model (BFM), due to the radial nature of the distribution networks [14–16]. On the basis of this formulation, second-order conic relaxation has been advocated in [17, 18] for convexification. The numerical performance of BFM is commonly regarded slightly superior to that of BIM in distribution networks.

This paper tackles the uncertainties by coordinating slow and fast controlling devices using BFM. A dual time-scale coordinated control scheme is proposed, as shown in Fig. 1.

In the case of the larger time-scale, here-and-now dispatch of slow controlling devices (including VRs and MSCs) is determined. This occurs on scales of tens of minutes or even hours (hereafter referred to as *slow control*). In the case of the smaller time-scale, the controlling device is activated every minute using a wait-and-see control method for reactive optimal power flow, e.g. reactive outputs of DGs and static VAr compensators (SVCs), are used to mitigate the impact of frequent voltage variations that occur due to uncertain demands and the output of the DGs (hereafter referred to as *fast control*). In the case of slow control, a robust VO (RVO) model is proposed to determine the operation of slow devices and guarantee that the subsequent fast controls can ensure the system's voltage security as long as the uncertain parameters vary within the predefined limits. As conventional deterministic optimisation models are suitable for fast control, this paper addresses a robust optimisation model used for slow control.

As shown in Fig. 1, the operating times for the slow controls should be optimally scheduled in advance. Some heuristic approaches have been proposed in previous work [19, 20]. This paper concentrates on how to generate optimal control strategies when the operating times are determined. Since the MADPTs of the slow controlling devices are considered when scheduling operating times, the sequential slow controls can be formulated as independent optimisation problems.

The main contributions of this paper include:

i. No literatures before have ever reported such a dual time-scale coordinated control scheme to reduce the uncertainty of load and DG for three-phase distribution networks. Different from [9] which is essentially based on scenario method, the coordination is directly cast as a multilevel robust optimisation problem in this paper. Both the convergence of the dual time-scale coordination and the optimality under uncertainties are guaranteed theoretically.
ii. An RVO model is developed to determine the operation of slow devices and guarantee that the subsequent fast controls can maintain the system's voltage security under specified uncertainties.

The remainder of this paper is organised as follows: in Section 2, the RVO model for slow control is formulated. Section 3 describes the solution methodology. Section 4 details the results of numerical simulations. These demonstrate the performance of the proposed algorithm. Section 5 concludes this paper.

2 RVO model

In this section, we describe deterministic and RVO models. First, we review a deterministic model using forecast loads and active DG outputs.

2.1 Deterministic model

For an ADN with N buses, where bus 1 denotes the point of common coupling, the reactive power optimisation problem is to find an optimal dispatch for the system equipment (e.g. VRs, MSCs, DGs, SVCs etc.). This should minimise losses whilst taking into account security constraints. Farivar and Low [17] showed that the non-convex branch flow in radial distribution networks can be convexified and that the deterministic model can be formulated as the following problem.

2.1.1 Objective function: We aim to minimise the active power loss of the network, i.e.

$$\min_{\beta,\,\kappa,\,Q_{\mathrm{C}},\,Q_{\mathrm{G}}} \quad \sum_{\varphi=a,\,b,\,c}\ \sum_{(i,\,j)\in\mathscr{E}} l_{ij}^{\varphi} r_{ij}^{\varphi} \tag{1}$$

2.1.2 DistFlow branch flow constraints in second-order conic programming (SOCP) form: In power distribution systems, DistFlow branch equations are typically used to describe the power flow. The equations were first proposed by Baran and Wu in [14] and later adopted by Low in [17] for relaxations and convexification

$$\sum_{i:\,i\to j}\left(P_{ij}^{\varphi}-l_{ij}^{\varphi}r_{ij}^{\varphi}\right)+P_{j}^{\varphi}=\sum_{k:\,j\to k}P_{jk}^{\varphi},\quad \forall j\in\mathscr{N},\quad \forall\varphi \tag{2}$$

$$\sum_{\substack{i:\,i\to j\\ \forall\varphi}}\left(Q_{ij}^{\varphi}-l_{ij}^{\varphi}x_{ij}^{\varphi}\right)+Q_{j}^{\varphi}-\beta_{j}^{\varphi}\bar{b}_{j}^{\varphi,\,C}v_{j}^{\varphi}=\sum_{k:\,j\to k}Q_{jk}^{\varphi},\quad \forall j\in\mathscr{N}, \tag{3}$$

$$v_{j}^{\varphi}=\kappa_{ij}^{\varphi,\,2}v_{i}^{\varphi}-2\left(r_{ij}^{\varphi}P_{ij}^{\varphi}+x_{ij}^{\varphi}Q_{ij}^{\varphi}\right)+\left(r_{ij}^{\varphi,\,2}+x_{ij}^{\varphi,\,2}\right)l_{ij}^{\varphi},\quad \forall(i,\,j)\in\mathscr{E},\quad \forall\varphi \tag{4}$$

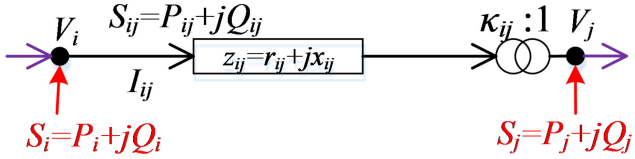

Fig. 2 *DistFlow BFM with VRs*

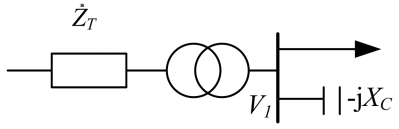

Fig. 3 *ULTC at substation side*

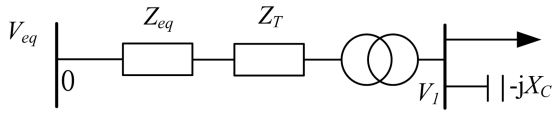

Fig. 4 *Illustration of Thevenin's equivalence for transmission network*

$$\left\| \begin{matrix} 2P_{ij}^{\varphi} \\ 2Q_{ij}^{\varphi} \\ l_{ij}^{\varphi}-v_i^{\varphi} \end{matrix} \right\|_2 \le l_{ij}^{\varphi}+v_i^{\varphi}, \quad \forall (i,j)\in\mathscr{E}, \quad \forall\varphi \tag{5}$$

$$P_j^{\varphi}=P_{\mathrm{G}j}^{\varphi}-P_{\mathrm{D}j}^{\varphi}, \quad \forall j\in\mathscr{N}, \quad \forall\varphi \tag{6}$$

$$Q_j^{\varphi}=Q_{\mathrm{G}j}^{\varphi}+Q_{\mathrm{C}j}^{\varphi}-Q_{\mathrm{D}j}^{\varphi}, \quad \forall j\in\mathscr{N}, \quad \forall\varphi \tag{7}$$

$$\kappa_{ij}^{\varphi}\in\mathscr{K}_{ij} \tag{8}$$

$$\mathscr{K}_{ij}=\begin{cases}\{K_{ij,1}, K_{ij,2}, \ldots, K_{ij,R}\}, & \text{if } (i,j)\in\mathscr{VR}\\ \{1.0\}, & \text{otherwise}\end{cases} \tag{9}$$

$$\beta_j^{\varphi}\in\mathscr{B}_j \tag{10}$$

$$\mathscr{B}_j=\begin{cases}\{0,1\}, & \text{if } j\in\mathscr{CB}\\ 0, & \text{otherwise}\end{cases} \tag{11}$$

Here, (2) is the conventional nodal active power balance constraint used in the DistFlow equations. Equation (3) extends the conventional nodal reactive power balance constraint by considering MSCs. Equation (4) is a general form of the voltage constraint that takes into account branches with VRs, as shown in Fig. 2. Equation (5) is the relaxed second-order conic constraint proposed in [17]. Equations (6) and (7) represent the net injected active and reactive powers for each bus, respectively. Equations (8) and (9) describe all allowable taps of branch ij; (10) and (11) specify allowable on–off decisions at bus i. Combined with (8)–(11), the branch flow equations in (3) and (4) provide a unified expression for the cases with or without MSCs and VRs.

2.1.3 Reference voltage constraint:

$$V_1^{\varphi}=V_{\mathrm{ref}}, \quad \forall\varphi \tag{12}$$

Equation (12) implies that the voltage of reference bus is set to reference voltage.

Remark 1: Actually this constraint does not make any assumption of constant voltage at reference bus. For some types of distribution networks, the substation voltage is controlled by an ULTC which is a discrete device and cannot keep the voltage V_1 exactly at the reference value (Fig. 3).

In this case, Thevenin's equivalence is performed from substation side toward transmission network. Since the topology of transmission network changes rarely, the Thevenin's equivalence parameters V_{eq}, Z_{eq} can be updated in an offline fashion. As shown in Fig. 4, the fictitious bus 0 can be regarded as a new 'reference bus', the voltage of which is equal to the V_{eq} (V_{eq} can be updated according to the power flow on transformer and V_1 before each calculation). The Thevenin's equivalence circuit can approximately represent the influence that the transmission network imposes on distribution network and the proposed algorithm still applies.

2.1.4 Security constraints:

$$\left|l_{ij}^{\varphi}\right| \le \bar{I}_{ij}^{\varphi,2}, \quad \forall (i,j)\in\mathscr{E}, \quad \forall\varphi \tag{13}$$

$$\underline{V}_i^{\varphi,2} \le v_i^{\varphi} \le \bar{V}_i^{\varphi,2}, \quad \forall i\in\mathscr{N}, \quad \forall\varphi \tag{14}$$

The security constraints for the current of branch ij are represented by (13). Voltage violation is prevented by introducing a voltage constraint (14).

2.1.5 Operating constraints of DGs and compensation devices:

$$\underline{Q}_{\mathrm{G}i}^{\varphi} \le Q_{\mathrm{G}i}^{\varphi} \le \bar{Q}_{\mathrm{G}i}^{\varphi}, \quad \forall i\in\mathscr{N}, \quad \forall\varphi \tag{15}$$

$$\underline{Q}_{\mathrm{C}i}^{\varphi} \le Q_{\mathrm{C}i}^{\varphi} \le \bar{Q}_{\mathrm{C}i}^{\varphi}, \quad \forall i\in\mathscr{N}, \quad \forall\varphi \tag{16}$$

The reactive powers of the DGs and SVCs are confined by (15) and (16).

2.2 Convexification of deterministic model

It is very difficult to obtain global optimal solutions of the non-convex deterministic model efficiently. Therefore, the cross-terms in (3) and (4) have to be relaxed.

2.2.1 Relaxation of MSCs: By introducing $\omega_j^{\varphi}=v_j^{\varphi}\beta_j^{\varphi}$, Ahmadi *et al.* [4] show that (3) is identical to

$$\sum_{i:i\to j}(Q_{ij}^{\varphi}-l_{ij}^{\varphi}x_{ij}^{\varphi})+Q_j^{\varphi}-\bar{b}_j^{\varphi,\mathrm{C}}\omega_j^{\varphi}=\sum_{k:j\to k}Q_{jk}^{\varphi}, \quad \forall j\in\mathscr{N}, \quad \forall\varphi \tag{17}$$

with additional constraints

$$v_j^{\varphi}-\bar{V}_j^{\varphi,2}(1-\beta_j^{\varphi}) \le \omega_j^{\varphi} \le v_j^{\varphi}-\underline{V}_j^{\varphi,2}(1-\beta_j^{\varphi}), \quad \forall j\in\mathscr{N}, \quad \forall\varphi \tag{18}$$

$$\underline{V}_j^{\varphi,2}\beta_j^{\varphi} \le \omega_j^{\varphi} \le \bar{V}_j^{\varphi,2}\beta_j^{\varphi}, \quad \forall j\in\mathscr{N}, \quad \forall\varphi \tag{19}$$

2.2.2 Exact linearisation of VR model: The intuitive idea is to approximate the original surface by a series of polyhedra. The approximation is exact in the case of discrete feasible set of tap settings for VRs, as shown in Fig. 5. By using the exact piecewise linearisation technique from [21], (4) can be rewritten as

$$\begin{aligned}\sum_{k=1}^{R-1}K_{ij,k}^{\varphi,2}(g_{ij,k}^{\varphi}\underline{V}_i^{\varphi,2}+h_{ij,k}^{\varphi}\bar{V}_i^{\varphi,2})-2(r_{ij}^{\varphi}P_{ij}^{\varphi}+x_{ij}^{\varphi}Q_{ij}^{\varphi})\\ +(r_{ij}^{\varphi,2}+x_{ij}^{\varphi,2})l_{ij}^{\varphi}-v_j^{\varphi}=0, \quad \forall (i,j)\in\mathscr{E}, \quad \forall\varphi\end{aligned} \tag{20}$$

with extra constraints

$$\sum_{k=1}^{R}(g_{ij,k}^{\varphi}+h_{ij,k}^{\varphi})=1 \tag{21}$$

$$\sum_{k=1}^{R-1}\delta_{ik}^{\varphi}=1 \tag{22}$$

$$0\le g_{ij,1}^{\varphi}, h_{ij,1}^{\varphi}\le\delta_{ij,1} \tag{23}$$

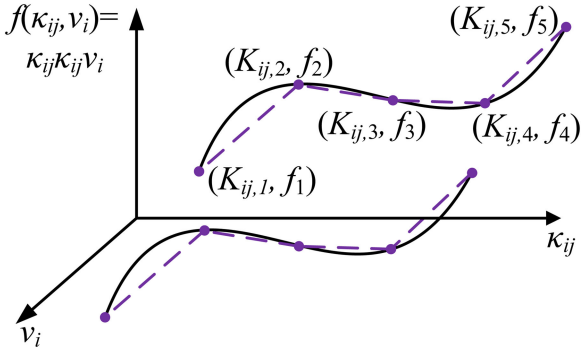

Fig. 5 *Piecewise linearisation of cross-term introduced by VRs*

$$0 \le g^{\varphi}_{ij,R},\ h^{\varphi}_{ij,R} \le \delta^{\varphi}_{ij,R-1} \tag{24}$$

$$0 \le g^{\varphi}_{ij,k},\ h^{\varphi}_{ij,k} \le \delta^{\varphi}_{ij,k} + \delta^{\varphi}_{ij,k-1}, \quad \forall k \in [2,\ R-1] \tag{25}$$

$$\delta^{\varphi}_{ij,k} \in \{0,\ 1\} \tag{26}$$

where δ_{ik} denotes the section of interest. Note that the allowable taps divide the function f into R sections, $g_{ij,k}$ and $h_{ij,k}$ are auxiliary variables that approximate the original function f. For details, please see [21].

2.2.3 Compact form of the convex deterministic VO (DVO) model: The convex deterministic model consists of an objective

$$\min_{\beta,\ \kappa,\ g,\ h,\ \delta,\ \omega,\ Q_C,\ Q_G} \quad \sum_{\varphi=a,\ b,\ c} \sum_{(i,\ j)\in\mathscr{E}} I^{\varphi}_{ij} r^{\varphi}_{ij} \tag{27}$$

with constraints (2), (17)–(19), (20)–(26) and (5)–(16). By defining an augmented vector $\boldsymbol{x} = (\beta,\ \kappa,\ g,\ h,\ \delta,\ \omega)$ that holds the decision variables for the MSCs and VRs, a vector $\boldsymbol{y} = (Q_C,\ Q_G,\ v,\ l_{ij},\ P_{ij},\ Q_{ij})^{\mathrm{T}}$ that relates the power flow and the dispatch of DGs and SVCs and a forecasted vector $\boldsymbol{d}_0 = (P_D,\ Q_D,\ Q_G)^{\mathrm{T}}$, this model can also be written in a compact form

$$\min_{\tilde{\boldsymbol{x}},\ \boldsymbol{y}} \quad \boldsymbol{b}^{\mathrm{T}}\boldsymbol{y} \tag{28}$$

$$s.t. \quad \boldsymbol{A}\boldsymbol{x} + \boldsymbol{B}\boldsymbol{y} + \boldsymbol{d}_0 = 0 \tag{29}$$

$$\boldsymbol{C}\boldsymbol{x} + \boldsymbol{D}\boldsymbol{y} \ge \boldsymbol{e} \tag{30}$$

$$\boldsymbol{x} \in \mathscr{X} \tag{31}$$

$$\| \boldsymbol{G}_l\boldsymbol{y} \|_2 \le \boldsymbol{g}_l^{\mathrm{T}}\boldsymbol{y}, \quad \forall l \in \mathscr{E} \tag{32}$$

$$\underline{\boldsymbol{y}} \le \boldsymbol{y} \le \bar{\boldsymbol{y}} \tag{33}$$

where (28) is equivalent to (27), (29) represents the power balance constraints (2), (17) and (20), (30) is identical to the inequality constraints (18) and (19), (31) is an expression for the constraints (8)–(11) and (21)–(26), (32) simplifies the expression of (5) and the security constraints in (13) and (14) and the reference constraint in (12) can be represented by (33).

2.3 Two-stage RVO model

In the deterministic model, neither the difference in time-scales among our devices nor the uncertainties in the loads and DG outputs is considered. In the robust model, it is assumed that the dispatch for the slow control (VRs and MSCs) is decided prior to the loads and active DG outputs of DGs occurring. For each instance of uncertain loads and DG outputs, the fast control (reactive outputs of SVCs and DGs) reduces network losses and prevents voltage violation. The first-stage dispatch of VRs and MSCs attempts to minimise the worst-case second-stage power loss, which can be formulated as the following two-stage robust model:

$$\min_{\boldsymbol{x}} \ \max_{\boldsymbol{d}\in\mathscr{D}} \ \min_{\boldsymbol{y}} \quad \boldsymbol{b}^{\mathrm{T}}\boldsymbol{y} \tag{34}$$

$$\text{s.t.} \quad \boldsymbol{A}\boldsymbol{x} + \boldsymbol{B}\boldsymbol{y} + \boldsymbol{d} = 0, \quad \forall \boldsymbol{d} \in \mathscr{D} \tag{35}$$

$$\boldsymbol{C}\boldsymbol{x} + \boldsymbol{D}\boldsymbol{y} \ge \boldsymbol{e}, \quad \forall \boldsymbol{d} \in \mathscr{D} \tag{36}$$

$$\| \boldsymbol{G}_l\boldsymbol{y} \|_2 \le \boldsymbol{g}_l^{\mathrm{T}}\boldsymbol{y}, \quad \forall l \in \mathscr{E}, \quad \forall \boldsymbol{d} \in \mathscr{D} \tag{37}$$

$$\underline{\boldsymbol{y}} \le \boldsymbol{y} \le \bar{\boldsymbol{y}}, \quad \forall \boldsymbol{d} \in \mathscr{D} \tag{38}$$

and (31).

The uncertainty set $\mathscr{D}$ is assumed to form a polyhedron. This guarantees that the column-and-constraint generation (C&CG) algorithm used to solve the proposed model converges after a finite number of iterations [22]. First, we calculate the optimal reactive power flow of a given schedule $\tilde{\boldsymbol{x}}$ of VRs and MSCs for a particular load and DG scenario $\boldsymbol{d}$, which replaces the forecasted value $\boldsymbol{d}_0$. This enables us to obtain the actual power losses. Next, the worst scenario where the optimal losses are maximised for a given dispatch of VRs and MSCs is obtained. Finally, our robust model finds an optimal way to dispatch the VRs and MSCs. This minimises the worst-case losses. It is ensured by (35)–(38) that power balance and security constraints are maintained when loads and active outputs of DGs fluctuate within the uncertainty set $\mathscr{D}$.

3 Solution methodology

The C&CG algorithm in [22] is used to solve the two-stage robust reactive power optimisation model. The distinctive feature of the proposed robust model is that the innermost problem is an SOCP, whereas the outermost problem is a mixed integer SOC program (MISOCP). The C&CG algorithm can be naturally extended for this robust reactive power optimisation model. The application of the algorithm is outlined as follows. The C&CG algorithm tries to solve the following extensive formulation of the proposed robust model:

$$\min_{\boldsymbol{x},\ \boldsymbol{y}(\boldsymbol{d}),\ \eta} \quad \eta \tag{39}$$

$$\text{s.t.} \quad \boldsymbol{b}^{\mathrm{T}}\boldsymbol{y}(\boldsymbol{d}) \le \eta \tag{40}$$

$$\eta \ge 0 \tag{41}$$

$$\boldsymbol{A}\boldsymbol{x} + \boldsymbol{B}\boldsymbol{y}(\boldsymbol{d}) + \boldsymbol{d} = 0, \quad \forall \boldsymbol{d} \in \mathscr{D} \tag{42}$$

$$\boldsymbol{C}\boldsymbol{x} + \boldsymbol{D}\boldsymbol{y}(\boldsymbol{d}) \ge \boldsymbol{e}, \quad \forall \boldsymbol{d} \in \mathscr{D} \tag{43}$$

$$\| \boldsymbol{G}_l\boldsymbol{y}(\boldsymbol{d}) \|_2 \le \boldsymbol{g}_l^{\mathrm{T}}\boldsymbol{y}(\boldsymbol{d}), \quad \forall l \in \mathscr{E}, \quad \forall \boldsymbol{d} \in \mathscr{D} \tag{44}$$

$$\underline{\boldsymbol{y}} \le \boldsymbol{y}(\boldsymbol{d}) \le \bar{\boldsymbol{y}}, \quad \forall \boldsymbol{d} \in \mathscr{D} \tag{45}$$

and (31).

The above problem has an infinite number of variables and constraints corresponding to each scenario $\boldsymbol{d}$.

3.1 Master problem

Owing to the infinite number of constraints (42)–(45), which are indexed by the uncertainty set $\mathscr{D}$, it is not possible to solve the above problem directly. The following reduced problem, where $\mathscr{D}$ is replaced by a finite subset, provides a lower bound for the robust model:

$$\min_{\boldsymbol{x},\ \boldsymbol{y}(t),\ \eta} \quad \eta \tag{46}$$

$$\text{s.t.} \quad \boldsymbol{b}\boldsymbol{y}(t) \le \eta, \quad \forall t = 1, 2, \ldots, t_0 \tag{47}$$

$$\boldsymbol{A}\boldsymbol{x} + \boldsymbol{B}\boldsymbol{y}(t) + \boldsymbol{d}(t) = 0, \quad \forall t = 1, 2, \ldots, t_0 \tag{48}$$

$$\boldsymbol{C}\boldsymbol{x} + \boldsymbol{D}\boldsymbol{y}(t) \ge \boldsymbol{e}, \quad \forall t = 1, 2, \ldots, t_0 \tag{49}$$

$$\| \boldsymbol{G}_l \boldsymbol{y}(t) \|_2 \le \boldsymbol{g}_l^{\mathrm{T}} \boldsymbol{y}(t), \quad \forall l, \quad \forall t = 1, 2, \ldots, t_0 \tag{50}$$

$$\underline{\boldsymbol{y}} \le \boldsymbol{y}(t) \le \bar{\boldsymbol{y}}, \quad \forall t = 1, 2, \ldots, t_0 \tag{51}$$

and (31).

where $\boldsymbol{d}(t) \in \mathcal{D}$, $t = 1, 2, \ldots, t_0$. The master problem is an MISOCP with binary variables in $\boldsymbol{x}$ and second-order conic constraints in (50).

3.2 Sub-problem

The next key step in the C&CG algorithm is to search for the worst-case scenario for the master problem and obtain an upper bound for the robust model. This is achieved by solving the following sub-problem:

$$\begin{aligned} \max_{\boldsymbol{d} \in \mathcal{D},\, \boldsymbol{\tau},\, \underline{\boldsymbol{\lambda}},\, \bar{\boldsymbol{\lambda}},\, \boldsymbol{\xi},\, \boldsymbol{\sigma}_l,\, \boldsymbol{\mu}_l,\, \boldsymbol{\zeta},\, \boldsymbol{\gamma}} \quad & -(\boldsymbol{A}\boldsymbol{x}^* + \underline{\boldsymbol{d}})^{\mathrm{T}} \boldsymbol{\tau} \\ & + \underline{\boldsymbol{y}}^{\mathrm{T}} \underline{\boldsymbol{\lambda}} - \bar{\boldsymbol{y}}^{\mathrm{T}} \bar{\boldsymbol{\lambda}} + (\boldsymbol{e} - \boldsymbol{C}\boldsymbol{x}^*)^{\mathrm{T}} \boldsymbol{\xi} - \Delta \boldsymbol{d}^{\mathrm{T}} \boldsymbol{\gamma} \end{aligned} \tag{52}$$

$$\text{s.t.} \quad \boldsymbol{\tau} - M(\boldsymbol{1} - \boldsymbol{\zeta}) \le \boldsymbol{\gamma} \le \boldsymbol{\tau} + M(\boldsymbol{1} - \boldsymbol{\zeta}) \tag{53}$$

$$\boldsymbol{B}^{\mathrm{T}} \cdot \boldsymbol{\tau} + \sum_l (\boldsymbol{G}_l^{\mathrm{T}} \boldsymbol{\sigma}_l + \mu_l \boldsymbol{g}_l) + \underline{\boldsymbol{\lambda}} - \bar{\boldsymbol{\lambda}} + \boldsymbol{D}^{\mathrm{T}} \cdot \boldsymbol{\xi} = \boldsymbol{b} \tag{54}$$

$$-M\boldsymbol{\zeta} \le \boldsymbol{\gamma} \le M\boldsymbol{\zeta} \tag{55}$$

$$\zeta_i \in \{0, 1\} \tag{56}$$

$$\| \boldsymbol{\sigma}_l \|_2 \le \boldsymbol{\mu}_l, \quad \forall l \tag{57}$$

$$\boldsymbol{\xi},\, \underline{\boldsymbol{\lambda}},\, \bar{\boldsymbol{\lambda}},\, \boldsymbol{\mu}_l \ge 0 \tag{58}$$

where $\boldsymbol{1}$ is a column vector whose elements are all equal to 1, M is a very large positive number (e.g. 10^6) and (53)–(55) are big-M constraints. Please see the Appendix for detailed derivation.

Table 1 Summary of the C&CG algorithm for RVO problem

1. **Initialisation** lower bound of network loss $\mathbf{LB} := 0$, and upper bound of network loss $\mathrm{UB} := \infty$, scenario index $t := 0$. Set tolerance level $\varepsilon > 0$

2. (2.1) Solve the master problem [(46)–(51) and (31)], which is a reduced problem considering typical worst-case scenario set, to get an optimal dispatch scheme $\boldsymbol{x}^*$ for MSCs and VRs and the corresponding network loss η^* (2.2) Update $\mathrm{LB} := \max\{\mathrm{LB}, \eta^*\}$ 3. The master problem sends $\boldsymbol{x}^*$ to the sub-problem

If $\mathrm{UB} - \mathrm{LB} < \varepsilon$, **End**

4. (4.1) For given $\boldsymbol{x}^*$, solve the sub-problem [(52)–(58)], which is a dual problem of the OPF, to obtain the optimal network loss $\eta(\boldsymbol{x}^*)$ and the corresponding worst-case scenario $\boldsymbol{d}^*$. The worst-case scenario $\boldsymbol{d}^*$ is consisting of the active power output of DGs and loads that maximise the network losses (4.2) Update $\mathrm{UB} := \min\{\mathrm{UB}, \eta(x^*)\}$ 5. The sub-problem sends newly generated worst-case scenario $\boldsymbol{d}^*$ to the master problem 6. The master problem updates its typical worst-case scenario set $\boldsymbol{d}(t+1) := \boldsymbol{d}^*$, creates variables $\boldsymbol{y}(t+1)$ and adds new constraints (35)–(38) of scenario $t+1$ to itself. 7. Update $t := t + 1$. Return to step 2

3.3 C&CG algorithm

The whole procedure to solve the two-stage robust reactive power optimisation problem is summarised in Table 1.

To be more readable, the schematic flowchart of the proposed algorithm is depicted in Fig. 6. The interaction between the master problem and the sub-problem is annotated over the arrow. The master problem solves a reduced problem considering typical worst-case scenario set. In this problem, the variables to be optimised are: the decision variables $\boldsymbol{x}$ which consists of on-and-off decision for the MSCs and the turn ratio for tap changer of VRs, the power flow variables (branch power and nodal voltage) $\boldsymbol{y}$ for typical extreme scenarios and the lower bound of network losses η. Then, master problem transfers the optimal dispatch $\boldsymbol{x}^*$ for slow control devices to sub-problem. After receiving the newly updated $\boldsymbol{x}^*$, the sub-problem simply solves the dual problem of optimal power flow in (52)–(58), searches the worst-case scenarios with the given $\boldsymbol{x}^*$. In the sub-problem, the main optimisation variables are worst-case scenario $\boldsymbol{d}^*$, i.e. the active power output of DGs and loads that maximise the network losses, while the Lagrangian multipliers $\boldsymbol{\tau}$, $\underline{\boldsymbol{\lambda}}$, $\bar{\boldsymbol{\lambda}}$, $\boldsymbol{\xi}$, $\boldsymbol{\sigma}_l$, $\boldsymbol{\mu}_l$, $\boldsymbol{\zeta}$, $\boldsymbol{\gamma}$ corresponding to constraints (61)–(64) are also obtained as byproduct. Moreover, finally the sub-problem sends the latest worst-case scenario $\boldsymbol{d}^*$ to master problem, and master problem updates its scenario index $t = t + 1$ and adds the latest worst-case scenario $\boldsymbol{d}^*$ (denoted by scenario t) to its typical worst-case scenario set. Meanwhile, constraints (47)–(51) corresponding to scenario t are also generated in the master problem. Moreover, the algorithm just starts another iteration when the master problem solves the augmented problem and sends back the latest optimal dispatch $\boldsymbol{x}^*$ again to the sub-problem.

The master problem updates the lower bound of the objectives, whereas the sub-problem updates the upper bound. The whole procedure terminates while the difference of these two bounds is sufficiently small.

Remark 2 (discussion of implementation): Most of the advanced application software for power system, e.g. voltage control, optimal power flow, depend on state estimation [23] which converts the real-time measurements of branch flow, injection power and voltage measurements into an estimate of the state vector. There are some interval prediction algorithms and the construction of uncertainty set $\mathcal{D}$ have been extensively studied; see, e.g. [24, 25]. To sum up, the proposed method depends on state estimation and forecasting intervals of DGs' output and load demands. The voltage control module should be deployed in control centre.

Remark 3 (comment on alternative approaches): There are mainly two alternative approaches that can address the voltage security issues:

i. The voltage difference from nominal can be included in the objective function of a deterministic method in (27), which can regulate voltage to some extent.

Since there are two terms, network losses and voltage difference, in the objective function, weighting is necessary. Parameter tuning is an open issue, not to mention the suboptimality by introducing voltage difference into objective function.

ii. The unsatisfied voltage constraints are relaxed by adding a voltage related term to the objective function with a large penalty.

In this solution, how to identify the unsatisfied voltage constraints is still an open question for an infeasible optimisation problem.

4 Simulation results

In this section, we outline results from numerical experiments on a real feeder from Shandong distribution system in China [6, 26], an IEEE 69-bus and a three-phase unbalanced IEEE 123-bus distribution systems [27] (Fig. 7–9). These were conducted to

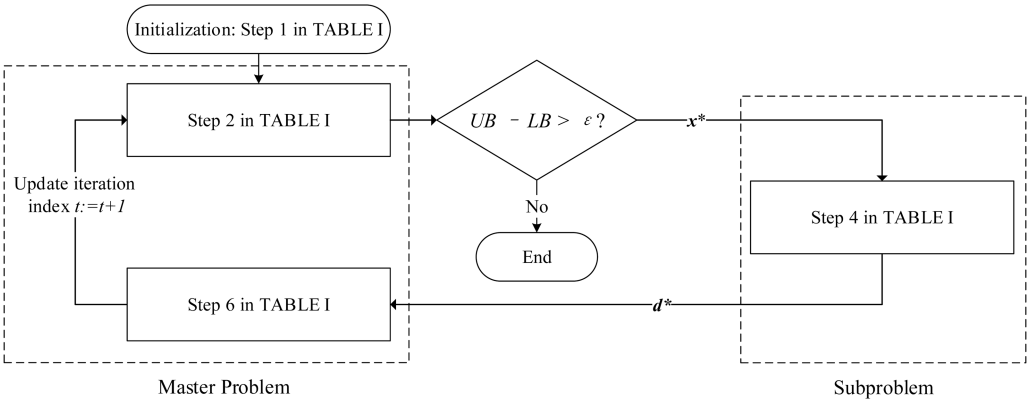

Fig. 6 *Flowchart of the proposed algorithm*

enable us to evaluate the performance of the proposed robust model.

In the IEEE 69-bus system, there are eight DGs, one VR and five MSCs. In the IEEE 123-bus system, there are ten DGs, two SVCs, one VR and five MSCs. DG at bus 68 is operated at phase B, whereas DGs at buses at 61 and 94 are operated at phase A and phase B. Other equipment is operated in three phase. Details of the configuration are listed in Table 2.

The admittance of the MSCs was set as 1.0 pu. The capacity of the SVCs was 0.3 pu. The capacity of the DGs was 0.3 pu for both active and reactive power generations. Suppose that the DGs operate in maximum power point tracking mode, which attempts to generate the maximum allowable active power, and the reactive power is optimised [28]. The allowable turn ratio of the VR lies in the interval [0.95, 1.05] with step length 0.01. The operational limits for voltage magnitude are 0.9 and 1.042 pu [29].

The algorithms: namely, the DVO model and the two-stage RVO model, were implemented using the MATLAB program and solved with IBM ILOG CPLEX software (ver. 12.5) [30]. The two-stage RVO consists of a stage of slow control and a stage of fast control. The test environment was a laptop with an Intel Core i5-3210M 2.50 GHz processor and 8 GB of random access memory.

The following uncertainty set is considered:

$$\mathscr{D} - = \left\{ \begin{pmatrix} P_{\mathrm{D}} \\ Q_{\mathrm{D}} \\ P_{\mathrm{G}} \end{pmatrix} \middle| \begin{array}{l} (1-\nu)P_{\mathrm{D}}^{\mathrm{Base}} \le P_{\mathrm{D}} \le (1+\nu)P_{\mathrm{D}}^{\mathrm{Base}} \\ (1-\nu)Q_{\mathrm{D}}^{\mathrm{Base}} \le Q_{\mathrm{D}} \le (1+\nu)Q_{\mathrm{D}}^{\mathrm{Base}} \\ (1-\nu)P_{\mathrm{G}}^{\mathrm{Base}} \le P_{\mathrm{G}} \le (1+\nu)P_{\mathrm{G}}^{\mathrm{Base}} \end{array} \right\} \tag{59}$$

where the base loads $P_{\mathrm{D}}^{\mathrm{Base}}$, $Q_{\mathrm{D}}^{\mathrm{Base}}$ were taken from the data in the standard test archive and the volatility is denoted as ν.

The simulation results are organised as follows. In Section 4.1, we first demonstrate the practical applicability issue of RVO. We use a real feeder in China and a scenario along with the base case to show the technical issues arising from DVO and how RVO can tackle with this issue. Then, both DVO and RVO were tested on a large number of scenarios generated by Monte Carlo simulation in Section 4.2, using two IEEE standard test archives. The results show that RVO can handle uncertainties in a single-time period. In Section 4.3, numerical tests were further performed in multiple-time period, and RVO can successively keep the voltage profiles within security region.

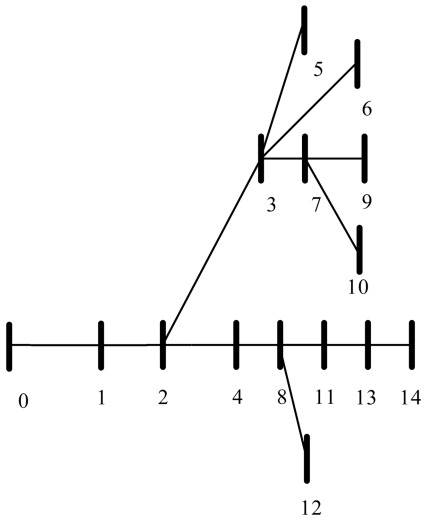

Fig. 7 *Real feeder from Shandong distribution system in China*

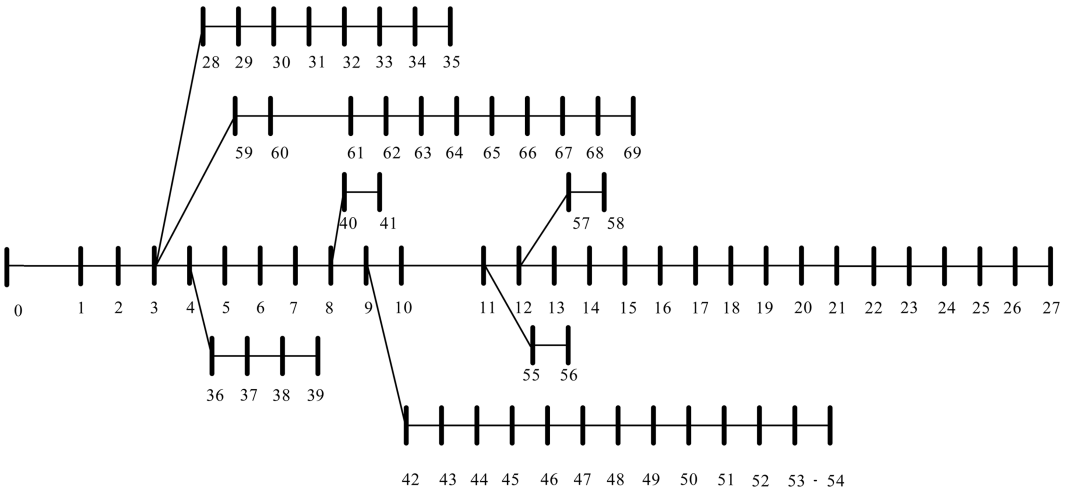

Fig. 8 *IEEE 69-bus distribution system*

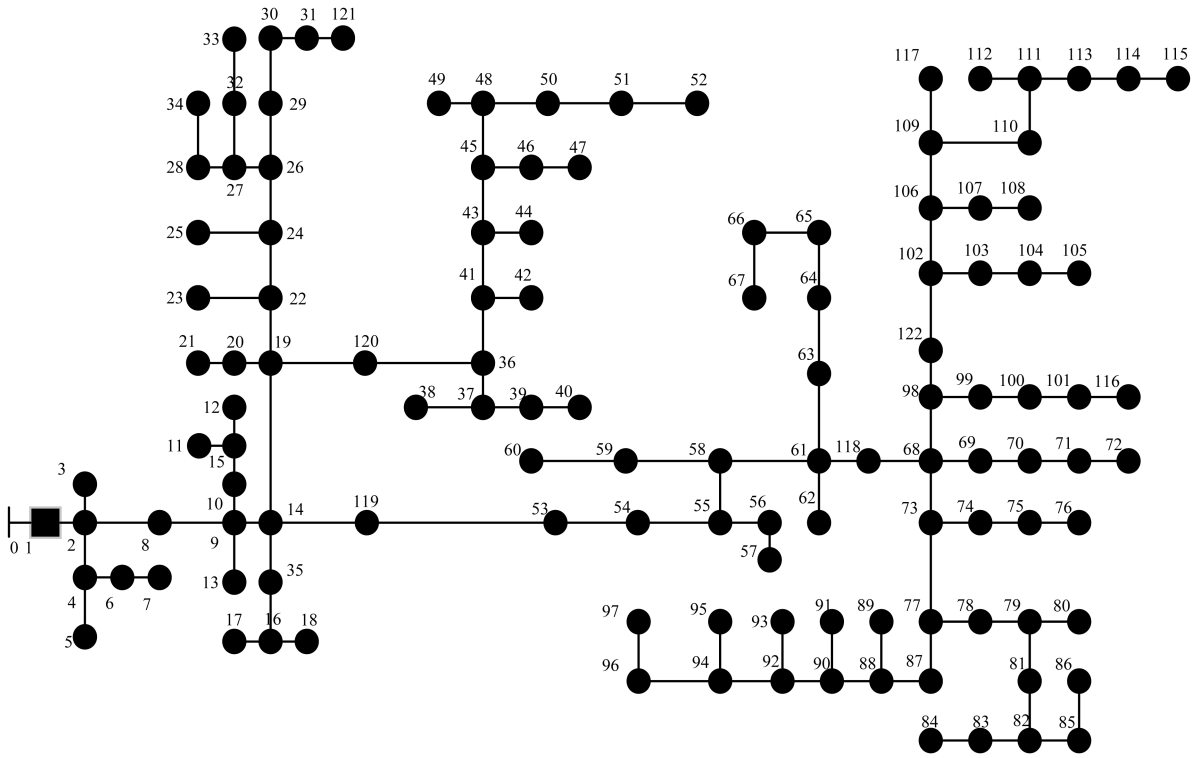

Fig. 9 *IEEE 123-bus distribution system*

Table 2 Configurations of test systems

System	Shandong 14-bus test feeder	IEEE 69-bus	IEEE 123-bus
DG	buses {5, 6, 7, 8, 9, 10, 11, 12, 13}	buses {19, 20, 26, 22, 54, 69, 34, 38}	buses {7, 12, 33, 47, 115, 98, 84, 19, 43, 61}
SVC	bus 14	—	buses {94, 68}
VR	line 3-7	line 10-11	line 58-61
MSC	buses {11, 12, 13, 14}	buses {5, 20, 27, 50, 25}	buses {4, 12, 19, 55, 93, 68, 43}

DGs, distributed generations; SVCs, static VAr compensators; VR, voltage regulator; and MSC, capacitor bank/MSC.

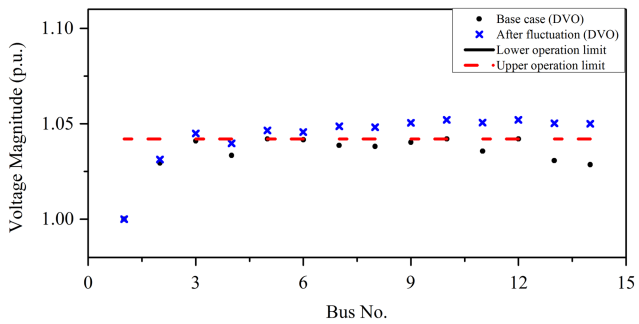

Fig. 10 *Simulated voltage magnitude of the convex DVO model in the Shandong test feeder*

4.1 Practical applicability of the proposed algorithm

The major drawback of DVO is first demonstrated through a real feeder from Shandong distribution system in China. Detailed data are all online available [26]. In this section, the base loads P_D^{Base}, Q_D^{Base} were taken from the data in [26] and the volatility ν is set as 50%. In the base case, though the voltage magnitudes of all buses did not violate upper bound, voltage violation occurred in buses {3, 5–14} after fluctuation of loads and DG outputs (50% loads and 150% DG active power outputs in comparison with the base case), as shown in Fig. 10. Moreover, this practical issue can be addressed by RVO, which can keep voltage security even after loads and DG outputs fluctuation as shown in Fig. 11.

Here, the reason why RVO differs from DVO is briefly discussed using the dispatch schedules generated by them in Table 3. Since DVO does not consider any uncertainties, its objective is to minimise network losses by increasing the voltages profile for the base-case scenario, which would probably encounter voltage violation after fluctuation of DGs. RVO is comparatively conservative when making control decisions for slow control devices by considering the worst-case scenario, which make the subsequent fast control has the capability to eliminate the voltage violations. The computation time is 0.096 s for DVO versus 0.327 s for RVO.

4.2 Comparison of handling uncertainties in a single-time period

In this section, the base loads P_D^{Base}, Q_D^{Base} were taken from the data in [27] and the volatility ν is set to 10%. In total, 100 Monte Carlo runs were conducted independently to generate scenarios.

In simulation, the DVO made optimal dispatches for VRs and MSCs, and achieved optimal reactive power flow for forecasted loads and DG outputs. However, the dispatch could not accommodate fluctuating loads and DG outputs, and the simulated voltage magnitude varied between the blue '×' and the black circle in Fig. 12. The slow control in the RVO considered all possibilities in the uncertainty set, and taken account each possible loads and active output of DGs. Therefore, the fast control enhanced optimality and feasibility. As a result, no voltage violation was observed in RVO simulations, which were prepared for the worst-case scenario, as shown in Fig. 13.

In Fig. 14, we see that the results for the IEEE 123-bus system were similar to those for the 69-bus system, except that voltage violation was more severe in this system with more DGs. Voltage violation was again eliminated by the RVO, as shown in Fig. 15. For the IEEE 69-bus system, the computation time is 1.958 s for RVO (versus 0.427 s for DVO). For the IEEE 123-bus system, the computation time is 3.870 s for RVO (versus 0.669 s for DVO).

The overall performance including the expectation of the network loss and failure rate (i.e. the possibility of voltage violation) is summarised in Table 4. Note that there are a number of infeasible cases in the DVO simulations. To enable direct

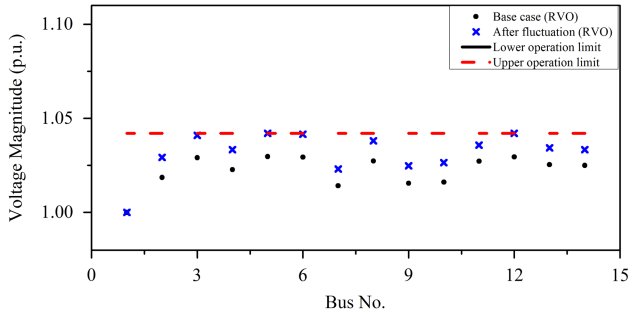

Fig. 11 *Simulated voltage magnitude of the two-stage RVO model in the Shandong test feeder*

Table 3 Control strategies for slow devices generated by RVO and DVO in Shandong test feeder (1: switch on, 0: switch off)

	Devices	Strategy	
		DVO	RVO
dispatch schedule	MSC11	1	0
	MSC12	0	0
	MSC13	1	0
	MSC14	1	1
	VR6	1.02	0.99

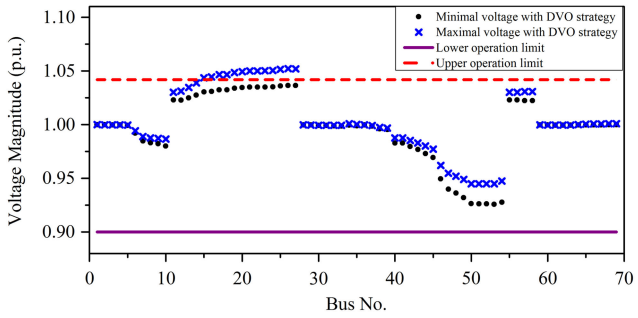

Fig. 12 *Simulated voltage magnitude of the convex DVO model in the IEEE 69-bus system*

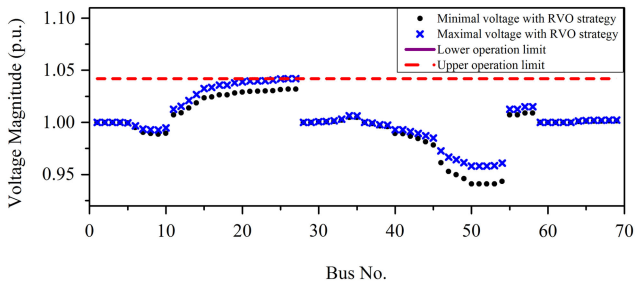

Fig. 13 *Simulated voltage magnitude of the two-stage RVO model in the IEEE 69-bus system*

comparisons, only expected losses for feasible cases are considered in DVO. This means that the infeasible cases have been removed prior to calculating the expected losses for DVO. RVO can prevent voltage violation in uncertain conditions with a reasonable extra cost of optimality in comparison with DVO.

The uncertainty set (59) can be adjusted by changing the volatility ν of demand and DG output variation. Table 5 shows the sensitivity of the minimum worst-case power losses of the RVO with respect to the different volatility of the uncertainty set in the IEEE 123-bus system. It is observed that the worst-case power losses increases as the size of the uncertainty set gets larger. The result is intuitive. A larger uncertainty set will make things worst and incur a higher power loss. The iterations required to converge are 2–3 steps, which shows that RVO is numerically stable.

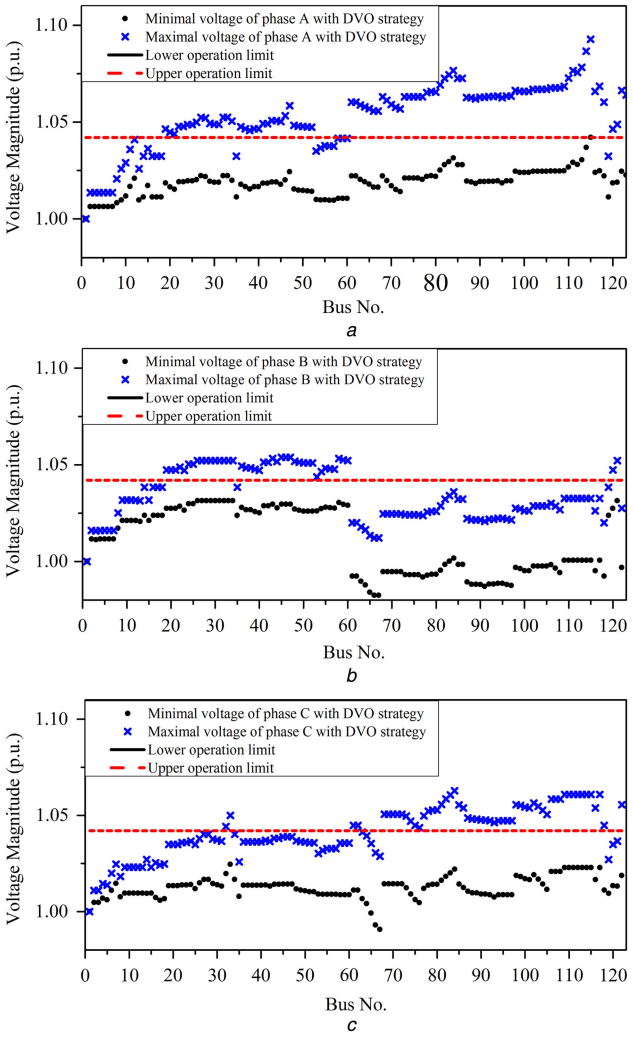

Fig. 14 *Simulated voltage magnitude of DVO in the IEEE 123-bus system for*
(a) Phase A, ***(b)*** Phase B, ***(c)*** Phase C

4.3 Comparison of handling uncertainties in multi-time period

The DVO and RVO were tested in multi-time period scenarios using the IEEE 123-bus system. Here, the DGs were assumed to be PV generators and their outputs were simulated using hybrid optimisation model for renewable energy (HOMER) software [31]. The standardised curves for the load and DG output are shown in Fig. 16. The 100% load level is the base load available in the test archive in [27], while the 100% PV output is the maximal capacity.

In the simulations, the DVO and RVO were compared using the load level and PV output level between 6 : 00 and 14 : 00. DVO made here-and-now decision for VRs, MSCs and optimal reactive power flow for current loads and DG outputs. When performing each slow control, an uncertainty set was constructed based on the extreme values of the injected active power over the whole test period. For each load and PV output, both algorithms adopted the fast controls. In both algorithms, the slow control interval was 2 h and fast control interval was 15 min.

A major reason for overvoltage is reverse power flow [29]. This problem is likely to occur in DVO when the growth of the PV outputs exceeds the growth of loads. This was especially the case in the period from 6 : 00 to 10 : 00 and from 11 : 00 to 12 : 00 in Fig. 16. Table 6 summarised the dispatch results for slow control using the DVO and RVO strategies for the IEEE 123-bus system. Fig. 17 depicts the number of overvoltage buses in the 123-bus system. Even with sequential fast controls, some buses operating beyond the upper voltage limits in the cases of DVO. However, in the cases of RVO, no voltage violations were observed for the entire time period investigated (6 : 00–14 : 00).

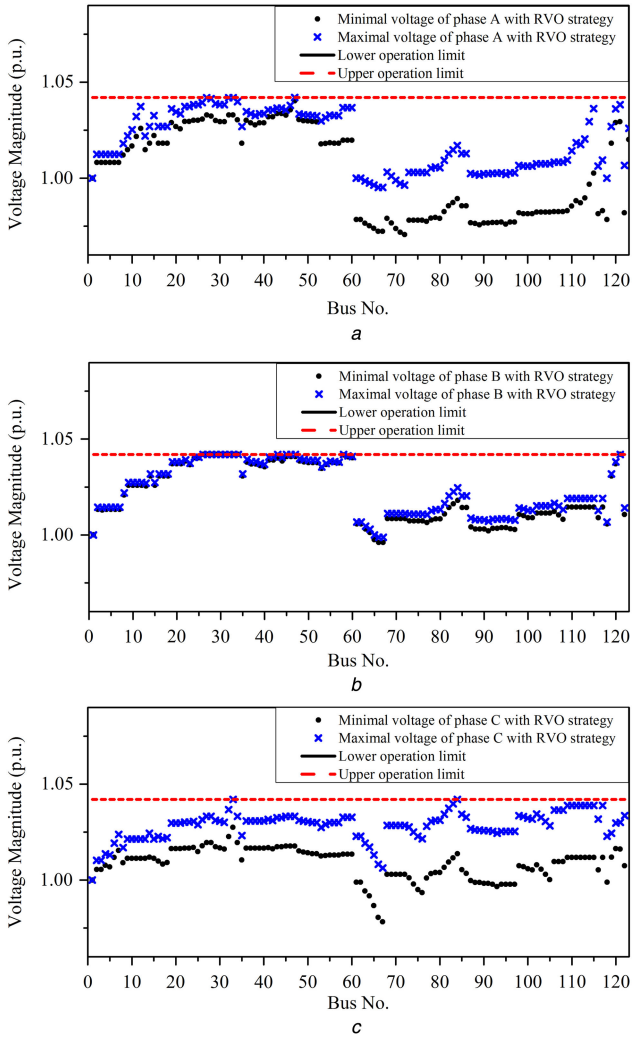

Fig. 15 *Simulated voltage magnitude of RVO in the IEEE 123-bus system for*
(a) Phase A, ***(b)*** Phase B, ***(c)*** Phase C

Table 4 Comparison of overall performance between DVO and RVO

System	DVO		RVO	
	$E[P_{loss}]$, kW	Failure rate, %	$E[P_{loss}]$, kW	Failure rate
69-bus	81.9	44	92.2	0
123-bus	212.0	68	213.0	0

DVO, convex DVO model; RVO, two-stage RVO model.

5 Conclusion

We described a dual time-scale coordinated robust reactive power and voltage optimisation model. This model can handle the uncertainties in predicted load and DG. The non-convex optimisation problem is first convexified using second-order conic relaxation for branch flow, piecewise linearisation for VRs and an equivalent transformation for MSCs. Then, a C&CG algorithm was used to solve the convexified robust model. The simulation results show that the solution of the deterministic model is not always feasible and voltage violations may occur. The robust model can ensure security with regard to all possible scenarios limited by the uncertainty sets with little compromise in terms of losses. Owing to

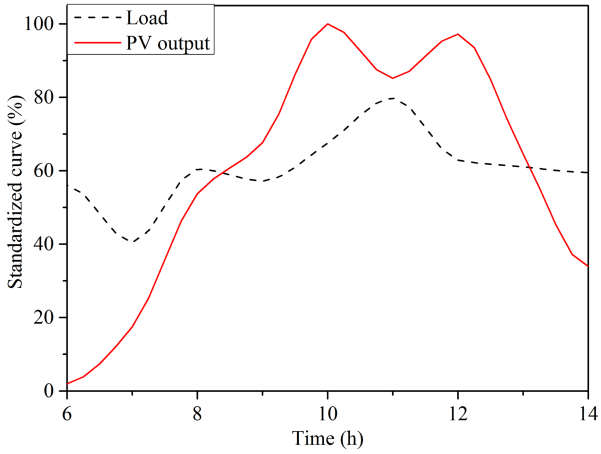

Fig. 16 *Standardised curves of the load and DG output*

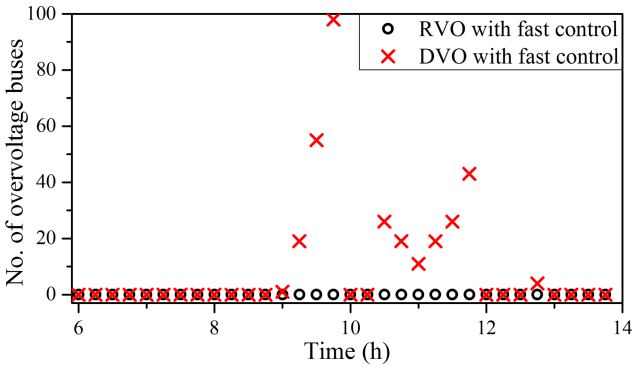

Fig. 17 *Evolution of overvoltage buses in the IEEE 123-bus system*

the MADPT constraints, the dispatch of the slow controlling devices should be formulated as a dynamic optimisation problem. To be applicable, this problem is always simplified into a sequence of independent static optimisation problems. This means that we need to schedule the operating times of the slow controlling devices in advance. Future research should address the question of exactly how to schedule these operating times. Development and implementation of a software that can be directly deployed in the operation centre is also an important future work.

6 Acknowledgments

This work was supported in part by the National Key Research and Development Plan of China (grant 2016YFB0900403) and in part by the National Science Foundation of China (grant 51477083).

Table 5 Comparison of RVO with different volatility of the uncertainty sets in IEEE 123-bus system

Volatility, ν	0.02	0.04	0.06	0.08	0.1
$E[P_{loss}]$, kW	208.9	210.1	211.2	212.0	213.0
iteration	2	2	2	3	3

Table 6 Control strategies for slow devices generated by RVO and DVO in IEEE 123-bus system (1: switch on, 0: switch off)

Strategy	Devices	Dispatch schedule			
		6 : 00	8 : 00	10 : 00	12 : 00
DVO	MSC4	1	0	0	1
	MSC12	1	0	0	0
	MSC19	1	0	0	0
	MSC55	0	0	0	0
	MSC93	0	0	0	0
	MSC68	0	0	0	0
	MSC43	1	1	1	1
	MSC5	1	0	1	0
	MSC119	0	0	0	0
	VR58	1.01	1.01	1.03	1.03
RVO	MSC4	0	1	0	0
	MSC12	1	1	0	1
	MSC19	1	1	0	1
	MSC55	0	0	0	0
	MSC93	0	0	0	0
	MSC68	0	0	0	0
	MSC43	0	1	1	1
	MSC5	0	0	0	0
	MSC119	0	0	0	0
	VR58	0.96	1.03	1.04	1.00

7 References

[1] Franchi, L., Innorta, M., Marannino, P., *et al.*: 'Evaluation of economy and/or security oriented objective functions for reactive power scheduling in large scale systems', *IEEE Trans. Power Appar. Syst.*, 1983, **PAS-102**, (10), pp. 3481–3488

[2] D'Adamo, C., Jupe, S., Abbey, C.: 'Global survey on planning and operation of active distribution networks – update of CIGRE C6.11 working group activities'. 20th Int. Conf. and Exhibition on Electricity Distribution – Part 1, 2009. CIRED 2009, 2009, pp. 1–4

[3] De Oliveira-De Jesus, P.M., Castronuovo, E.D., Ponce de Leao, M.T.: 'Reactive power response of wind generators under an incremental network-loss allocation approach', *IEEE Trans. Energy Convers.*, 2008, **23**, (2), pp. 612–621

[4] Ahmadi, H., Marti, J.R., Dommel, H.W.: 'A framework for volt–VAr optimization in distribution systems', *IEEE Trans. Smart Grid*, 2015, **6**, (3), pp. 1473–1483

[5] Zhang, B., Lam, A.Y.S., Dominguez-Garcia, A.D., *et al.*: 'An optimal and distributed method for voltage regulation in power distribution systems', *IEEE Trans. Power Syst.*, 2015, **30**, (4), pp. 1714–1726

[6] Zheng, W., Wu, W., Zhang, B., *et al.*: 'A fully distributed reactive power optimization and control method for active distribution networks', *IEEE Trans. Smart Grid*, 2015, **PP**, (99), p. 1

[7] Saric, A.T., Stankovic, X., A. M., : 'A robust algorithm for volt/Var control'. Power Systems Conf. and Exposition, 2009. PSCE '09, 2009, pp. 1–8

[8] Wang, Y., Wu, W., Zhang, B., *et al.*: 'Robust voltage control model for active distribution network considering PVs and loads uncertainties'. 2015 IEEE Power & Energy Society General Meeting, 2015, pp. 1–5

[9] Daratha, N., Das, B., Sharma, J.: 'Robust voltage regulation in unbalanced radial distribution system under uncertainty of distributed generation and loads', *Int. J. Electr. Power Energy Syst.*, 2015, **73**, pp. 516–527

[10] Gayme, D., Topcu, U.: 'Optimal power flow with large-scale storage integration', *IEEE Trans. Power Syst.*, 2013, **28**, pp. 709–717

[11] Lavaei, J., Low, S.H.: 'Zero duality gap in optimal power flow problem', *IEEE Trans. Power Syst.*, 2012, **27**, pp. 92–107

[12] Molzahn, D.K., Lesieutre, B.C., DeMarco, C.L.: 'A sufficient condition for global optimality of solutions to the optimal power flow problem', *IEEE Trans. Power Syst.*, 2014, **29**, pp. 978–979

[13] Lesieutre, B.C., Molzahn, D.K., Borden, A.R., *et al.*: 'Examining the limits of the application of semidefinite programming to power flow problems'. 2011 49th Annual Allerton Conf. on Communication, Control, and Computing (Allerton), 2011, pp. 1492–1499

[14] Baran, M.E., Wu, F.F.: 'Network reconfiguration in distribution systems for loss reduction and load balancing', *IEEE Trans. Power Deliv.*, 1989, **4**, (2), pp. 1401–1407

[15] Baran, M.E., Wu, F.F.: 'Optimal sizing of capacitors placed on a radial distribution system', *IEEE Trans. Power Deliv.*, 1989, **4**, pp. 735–743

[16] Esposito, A.G., Ramos, E.R.: 'Reliable load flow technique for radial distribution networks', *IEEE Trans. Power Syst.*, 1999, **14**, pp. 1063–1069

[17] Farivar, M., Low, S.H.: 'Branch flow model: relaxations and convexification (part I)', *IEEE Trans. Power Syst.*, 2013, **28**, (3), pp. 2554–2564

[18] Farivar, M., Low, S.H.: 'Branch flow model: relaxations and convexification (part II)', *IEEE Trans. Power Syst.*, 2013, **28**, pp. 2565–2572

[19] Wu, W., Zhang, B., Lo, K.L.: 'Capacitors dispatch for quasi minimum energy loss in distribution systems using a loop-analysis based method', *Int. J. Electr. Power Energy Syst.*, 2010, **32**, (6), pp. 543–550

[20] Li, Z., Wu, W., Zhang, B., *et al.*: 'Adjustable robust real-time power dispatch with large-scale wind power integration', *IEEE Trans. Sustain. Energy*, 2015, **6**, (2), pp. 357–368

[21] Liu, B., Liu, F., Mei, S., *et al.*: 'Optimal reactive power flow with exact linearized transformer model in distribution power networks'. 2015 27th Chinese Control and Decision Conf. (CCDC), 2015, pp. 5562–5567

[22] Zeng, B., Zhao, L.: 'Solving two-stage robust optimization problems using a column-and-constraint generation method', *Oper. Res. Lett.*, 2013, **41**, (5), pp. 457–461

[23] Zheng, W., Wu, W., Gomez-Exposito, A., *et al.*: 'Distributed robust bilinear state estimation for power systems with nonlinear measurements', *IEEE Trans. Power Syst.*, 2016, **PP**, p. 1

[24] Kavousi-Fard, A., Khosravi, A., Nahavandi, S.: 'A new fuzzy-based combined prediction interval for wind power forecasting', *IEEE Trans. Power Syst.*, 2016, **31**, pp. 18–26

[25] Zhang, G., Wu, Y., Wong, K.P., *et al.*: 'An advanced approach for construction of optimal wind power prediction intervals', *IEEE Trans. Power Syst.*, 2015, **30**, pp. 2706–2715

[26] Distribution system in Shandong province, China. Available at https://www.drive.google.com/file/d/0BzVXltCTbTuyZU1aY0MzVUZGTGc/view?usp=sharing

[27] Distribution Test Feeders. Available at http://www.ewh.ieee.org/soc/pes/dsacom/testfeeders/

[28] Esram, T., Chapman, P.L.: 'Comparison of photovoltaic array maximum power point tracking techniques', *IEEE Trans. Energy Convers.*, 2007, **22**, (2), pp. 439–449

[29] Wang, Y., Zhang, P., Li, W., *et al.*: 'Online overvoltage prevention control of photovoltaic generators in microgrids', *IEEE Trans. Smart Grid*, 2012, **3**, (4), pp. 2071–2078

[30] Cplex. Available at http://www-01.ibm.com/software/integration/optimization/cplexoptimizer/

[31] HOMER. Available at http://www.nrel.gov/docs/fy04osti/35406.pdf

8 Appendix

Derivation of sub-problem: For the given dispatch scheme $\boldsymbol{x}^*$ of VRs and MSCs, the original sub-problem can be formulated as follows:

$$\eta(\boldsymbol{x}^*) = \max_{\boldsymbol{d} \in \mathcal{D}} \min_{\boldsymbol{y}} \quad \boldsymbol{b}^{\mathrm{T}}\boldsymbol{y} \tag{60}$$

$$\text{s.t.} \quad \boldsymbol{B}\boldsymbol{y} + \boldsymbol{d} = -\boldsymbol{A}\boldsymbol{x}^*, \quad (\boldsymbol{\tau}) \tag{61}$$

$$\boldsymbol{D}\boldsymbol{y} \geq \boldsymbol{e} - \boldsymbol{C}\boldsymbol{x}^*, \quad (\boldsymbol{\xi}) \tag{62}$$

$$\| \boldsymbol{G}_l \boldsymbol{y}(t) \|_2 \leq \boldsymbol{g}_l^{\mathrm{T}} \boldsymbol{y}(t), \quad \forall l \ (\boldsymbol{\sigma}_l \cdot \boldsymbol{\mu}_l) \tag{63}$$

$$\underline{\boldsymbol{y}} \leq \boldsymbol{y} \leq \bar{\boldsymbol{y}}, \quad (\underline{\boldsymbol{\lambda}}, \bar{\boldsymbol{\lambda}}) \tag{64}$$

The optimal objective value of this sub-problem is the worst-case network losses for a given dispatch scheme $\boldsymbol{x}^*$. Hence, it can be used to estimate an upper bound for the robust model. This two-level max–min problem cannot be solved directly. Therefore, we convert the inner conic problem. The Lagrangian function of the inner problem is (see (65)) with $\boldsymbol{\nu}_l, \underline{\boldsymbol{\lambda}}, \bar{\boldsymbol{\lambda}}, \boldsymbol{\xi} \geq 0$.

The dual problem can be formulated as

$$\max_{\boldsymbol{d}, \boldsymbol{\sigma}_l, \underline{\boldsymbol{\lambda}}, \bar{\boldsymbol{\lambda}}, \boldsymbol{\xi}, \boldsymbol{\mu}_l} \inf_{\boldsymbol{y}, \boldsymbol{o}_l, \omega_l} L(\boldsymbol{y}, \boldsymbol{d}, \boldsymbol{\sigma}_l, \underline{\boldsymbol{\lambda}}, \bar{\boldsymbol{\lambda}}, \boldsymbol{\xi}, \boldsymbol{\mu}_l) \tag{66}$$

The minimisation over $\boldsymbol{y}$ and ω_l is bounded if and only if

$$\boldsymbol{B}^{\mathrm{T}} \cdot \boldsymbol{\tau} + \sum_l (\boldsymbol{G}_l^{\mathrm{T}} \boldsymbol{\sigma}_l + \mu_l \boldsymbol{g}_l) + \underline{\boldsymbol{\lambda}} - \bar{\boldsymbol{\lambda}} + \boldsymbol{D}^{\mathrm{T}} \cdot \boldsymbol{\xi} = \boldsymbol{b} \tag{67}$$

$$\mu_l = \nu_l, \quad \forall l \tag{68}$$

$$\| \boldsymbol{\sigma}_l \|_2 \leq \boldsymbol{\mu}_l, \quad \forall l \tag{69}$$

To minimise over $\boldsymbol{o}_l$, note that

$$\inf_{\boldsymbol{o}_l} \boldsymbol{\sigma}_l^{\mathrm{T}} \boldsymbol{o}_l + \nu_l \| \boldsymbol{o}_l \|_2 = \begin{cases} 0, & \| \boldsymbol{\sigma}_l \|_2 \leq \nu_l \\ -\infty, & \text{otherwise} \end{cases} \tag{70}$$

The Lagrangian dual function is

$$\theta(\boldsymbol{\sigma}_l, \underline{\boldsymbol{\lambda}}, \bar{\boldsymbol{\lambda}}, \boldsymbol{\xi}, \mu_l, \nu_l) = \begin{cases} -(\boldsymbol{A}x^* + \boldsymbol{d})^{\mathrm{T}} \boldsymbol{\tau} + \underline{\boldsymbol{y}}^{\mathrm{T}} \underline{\boldsymbol{\lambda}} & \text{if } \| \boldsymbol{\sigma}_l \|_2 \leq \nu_l, \\ -\bar{\boldsymbol{y}}^{\mathrm{T}} \bar{\boldsymbol{\lambda}} + (\boldsymbol{e} - \boldsymbol{C}x^*)^{\mathrm{T}} \boldsymbol{\xi}, & (61) \text{ and } (62) \\ -\infty, & \text{otherwise} \end{cases} \tag{71}$$

which leads to the dual problem in a monolithic form

$$\max_{\boldsymbol{d} \in \mathcal{D}, \boldsymbol{\tau}, \underline{\boldsymbol{\lambda}}, \bar{\boldsymbol{\lambda}}, \boldsymbol{\xi}, \boldsymbol{\sigma}_l, \boldsymbol{\mu}_l} -(\boldsymbol{A}\boldsymbol{x}^* + \boldsymbol{d})^{\mathrm{T}} \boldsymbol{\tau} + \underline{\boldsymbol{y}}^{\mathrm{T}} \underline{\boldsymbol{\lambda}} - \bar{\boldsymbol{y}}^{\mathrm{T}} \bar{\boldsymbol{\lambda}} + (\boldsymbol{e} - \boldsymbol{C}\boldsymbol{x}^*)^{\mathrm{T}} \boldsymbol{\xi} \tag{72}$$

$$\text{s.t.} \quad \boldsymbol{B}^{\mathrm{T}} \cdot \boldsymbol{\tau} + \sum_l (\boldsymbol{G}_l^{\mathrm{T}} \boldsymbol{\sigma}_l + \mu_l \boldsymbol{g}_l) + \underline{\boldsymbol{\lambda}} - \bar{\boldsymbol{\lambda}} + \boldsymbol{D}^{\mathrm{T}} \cdot \boldsymbol{\xi} = \boldsymbol{b} \tag{73}$$

$$\| \boldsymbol{\sigma}_l \|_2 \leq \boldsymbol{\mu}_l, \quad \forall l \tag{74}$$

$$\boldsymbol{\xi}, \underline{\boldsymbol{\lambda}}, \bar{\boldsymbol{\lambda}}, \quad \boldsymbol{\mu}_l \geq 0 \tag{75}$$

The objective function is linear except for the bilinear term $\boldsymbol{d}^{\mathrm{T}} \boldsymbol{\tau}$, and the constraints are all in SOCP form. With the assumption that the uncertainty set $\mathcal{D}$ is polyhedral, the extreme points of $\mathcal{D}$ can be described by a set of auxiliary binary variables and linear constraints. By introducing big-M constraints, the bilinear term can be linearised, which can enable us to transform the sub-problem into an MISOCP. When $\boldsymbol{d}$ fluctuates within the interval $[\underline{\boldsymbol{d}}, \bar{\boldsymbol{d}}]$, introducing an auxiliary binary vector $\boldsymbol{\zeta}$ that satisfies $d_i = \underline{d}_i + \zeta_i \Delta d_i$ element-wise and an auxiliary variable $\gamma_i = \zeta_i \tau_i$, the above bilinear program is equivalent to the MISOCP listed in (52)–(58).

$$\begin{aligned} L(\boldsymbol{y}, \boldsymbol{o}_l, \omega_l, \boldsymbol{\sigma}_l, \underline{\boldsymbol{\lambda}}, \bar{\boldsymbol{\lambda}}, \boldsymbol{\xi}, \boldsymbol{\mu}_l, \nu_l) &= \boldsymbol{b}^{\mathrm{T}} \boldsymbol{y} - \boldsymbol{\tau}^{\mathrm{T}} (\boldsymbol{A}x^* + \boldsymbol{B}\boldsymbol{y} + \boldsymbol{d}) - \sum_l \boldsymbol{\sigma}_l^{\mathrm{T}} (\boldsymbol{G}_l \boldsymbol{y} - \boldsymbol{o}_l) \\ &\quad - \sum_l \mu_l (\boldsymbol{g}_l^{\mathrm{T}} \boldsymbol{y} - \omega_l) - \sum_l \nu_l (\omega_l - \| \boldsymbol{o}_l \|_2) - \underline{\boldsymbol{\lambda}}^{\mathrm{T}} (\boldsymbol{y} - \underline{\boldsymbol{y}}) \\ &\quad - \bar{\boldsymbol{\lambda}}^{\mathrm{T}} (\bar{\boldsymbol{y}} - \boldsymbol{y}) - \boldsymbol{\xi}^{\mathrm{T}} (\boldsymbol{D}\boldsymbol{y} + \boldsymbol{C}x^* - \boldsymbol{e}) \\ &= [\boldsymbol{b}^{\mathrm{T}} - \boldsymbol{\tau}^{\mathrm{T}} \boldsymbol{B} - \sum_l (\boldsymbol{\sigma}_l^{\mathrm{T}} \boldsymbol{G}_l + \mu_l \boldsymbol{g}_l^{\mathrm{T}}) - \underline{\boldsymbol{\lambda}}^{\mathrm{T}} + \bar{\boldsymbol{\lambda}}^{\mathrm{T}} - \boldsymbol{\xi}^{\mathrm{T}} \boldsymbol{D}] \boldsymbol{y} \\ &\quad - \boldsymbol{\tau}^{\mathrm{T}} (\boldsymbol{A}x^* + \boldsymbol{d}) + \underline{\boldsymbol{\lambda}}^{\mathrm{T}} \underline{\boldsymbol{y}} - \bar{\boldsymbol{\lambda}}^{\mathrm{T}} \bar{\boldsymbol{y}} + \sum_l (\boldsymbol{\sigma}_l^{\mathrm{T}} \boldsymbol{o}_l + \nu_l \| \boldsymbol{o}_l \|_2) \\ &\quad + \sum_l (\mu_l - \nu_l) \omega_l - \boldsymbol{\xi}^{\mathrm{T}} (\boldsymbol{C}x^* - \boldsymbol{e}) \end{aligned} \tag{65}$$